A Low-Speed, High-Torque, Direct-Drive Permanent Magnet Generator For Wind Turbines

W. Wu
CSIRO Telecommunications & Industrial Physics
PO Box 218, Lindfiled NSW 2070
Australia

V.S. Ramsden
Faculty of Engineering, UTS
PO Box 123, Broadway
NSW 2007
Australia

T. Crawford, G. Hill
Westwind Turbines Pty Ltd
29 Owen Road, Kelmscott
Western Australia 6111
Australia

***Abstract*-There is a market for small, efficient and cost-effective wind generators for mini-grid and remote power systems. Direct-drive permanent magnet generators have become very attractive for this application. This paper describes the improvements achieved in an outer-rotor direct-drive permanent magnet generator by using finite element analysis and optimisation techniques. The starting torque of the generator is studied. An optimisation routine for the design, including magnetic finite element analysis and lumped-parameter thermal model, is presented. A prototype for 20 kW, 211 rpm generator was built. The test results with a resistive load confirm the satisfactory operation of the generator. Compared with the previous prototype, the new design has lower mass, lower starting torque and improved efficiency.**

I. Introduction

Traditionally wind turbine generators have used gearboxes and pitch control to allow constant high-speed generation under varying wind speed conditions. In recent years contemporary power electronics of high efficiency, high reliability and decreasing cost offers the option to change the power frequency out of the generator to match the system frequency, which leads to the idea of variable-speed direct-drive generators. A number of alternative concepts have been proposed for direct-drive electrical generators for use in grid-connected or stand-alone wind turbines [1,2]. Compared to a conventional gearbox-coupled wind turbine generator, a direct-drive generator has reduced overall size, lower installation and maintenance cost, a flexible control method and quick response to wind fluctuations and load variation.

A direct-drive generator must be light and efficient to minimise the requirements for the tower structure and to maximise electrical power extracted from the wind. For small wind turbines, direct-drive permanent magnet generators have become very attractive because of their high efficiency, high power density and robust rotor structure. The attractiveness of direct-drive permanent magnet generators is further enhanced by improvements of permanent magnet characteristics and decrease of material prices. Some direct-drive examples are Enercon (E12, 30 kW), Proven (2.5 kW), LMW (2.5-10 kW) and Venco-Westwind (2.5-10 kW) [3].

A joint effort to develop a 20 kW low-speed, high-torque, direct-drive permanent magnet generator for wind turbines was initiated by the University of Technology Sydney (UTS) and Commonwealth Scientific and Industrial Research Organisation (CSIRO) in conjunction with the Australian Cooperative Research Centre for Renewable Energy (ACRE) and Venco-Westwind. A non-optimised, 48-pole, 170 rpm prototype was constructed by Venco-Westwind earlier [4]. It features a radial-flux, slotted-stator topology with outer-rotor and surface-mounted Nd-Fe-B magnets, as shown in Fig. 1. The magnets are bonded to the inner surface of a steel drum that rotates around a stationary stator with conventional three-phase windings. An advantage of this arrangement is that the centrifugal force of the rotating magnets applies a pressure to the bonding media, therefore increasing the reliability of the glued joint. Also the blades of the wind turbine are directly mounted on the front surface of the outer-rotor drum, which leads to a simple assembly process, as shown in Figs. 15 and 16.

This paper describes the improved design of the second prototype by using finite element analysis and computer search techniques. Section II considers starting torque. The analysis of the direct-drive permanent magnet generator is given in Section III. Section IV discusses the design optimisation and compares designs for several numbers of poles, and several lamination and magnet materials. In Section V, test results of the second prototype are compared with predicted performance. The conclusions are summarised in Section VI.

II. Starting Torque

The starting torque of a permanent magnet generator is the total torque including the peak cogging torque, hysteresis torque, and the torque necessary to overcome the bearing and seal friction of the generator. Hysteresis torque arises from the hysteresis loss of the generator. The cogging torque is a dominent component, which is inherently generated from the interaction of the magnets with the stator teeth.

For a direct-drive wind generator, the starting torque is an important design issue because high starting torque prevents operation at cut-in wind speed. As a consequence, it is necessary to reduce the starting torque to acceptable values.

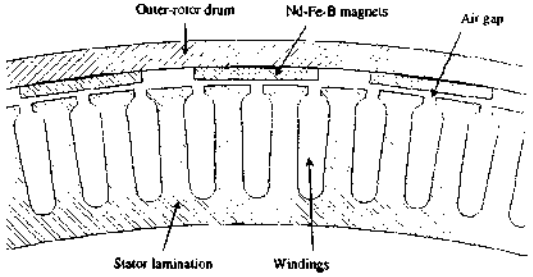

Fig. 1 Layout of the direct-drive permanent magnet generator

0-7803-6401-5/00/$10.00 © 2000 IEEE

The cogging torque can be calculated directly for different rotor positions, when the stator winding carries no current and the remanence of the magnet is known. Since the magnet remanence is temperature dependent, the cogging torque varies with the operating temperature of the generator. The maximum cogging torque occurs when the rotor temperature is at room temperature.

The cogging torque is affected by air gap length, slot wedge material, skew, magnet pole arc ratio, and slot opening width etc. For the first prototype, if the air gap is increased from 1.0 mm to 1.4 mm, the peak cogging torque is reduced from 62.6 Nm to 26.0 Nm. By using a magnetic slot wedge, the cogging torque can be reduced further from 26.0 Nm to 5.0 Nm. When the stator slot is skewed by one tooth width as used in the first prototype, the peak cogging torque decreases from 62.6 Nm to 11.8 Nm for an air gap of 1.0 mm. The cogging torque is very sensitive to the pole arc ratio as shown in Fig. 2(a). With a decrease of 0.72 to 0.6 of pole arc ratio, the peak cogging torque increases over 10 times. The slot opening width also affects the cogging torque. Fig. 2(b) shows the variation of peak cogging torque against the slot opening width.

It can be seen that there are a number of ways to reduce cogging torque, ie using a longer air gap, a magnetic slot wedge, slot skewing, and optimum magnet pole arc ratio and slot opening width. For the same output power, the use of a larger air gap may increase the thickness of the magnet. The use of a magnetic slot wedge increases the flux leakage between adjacent poles and reduces the output power of the generator. When the slots are skewed by one slot pitch, the cogging torque should be ideally reduced to zero, but the output is also reduced. The most effective solutions for cogging torque reduction are the adjustment of the magnet arc width and the slot opening width.

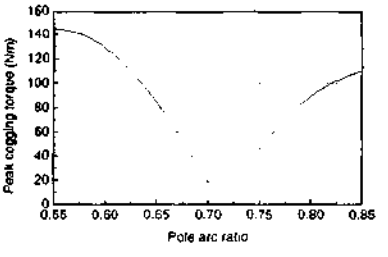

(a) Peak cogging torque against pole arc ratio

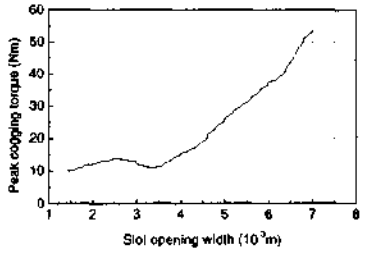

(b) Peak cogging torque against slot opening width

Fig. 2 Peak cogging torque

Therefore, optimising magnet arc and slot opening width to give a minimum cogging torque was used in the improved design.

III. Performance Analysis

The calculation of the operating characteristics of the generator is based on a finite element analysis of the magnetic field and a lumped-parameter circuit analysis of the thermal behaviour. The characteristics of the generator are predicted for fixed or variable speed operation under a balanced resistive load.

A. Back emf and synchronous reactance

The back emf is calculated from the variation of the flux linkage with the stator coil while the rotor turns. Fig. 3 compares the predicted and measured emf for the first prototype. Without skewed slots, the phase emf waveform shows a small dip in the middle, which is attributed to the effect of the slot opening and deep slots. The phase emf waveform becomes trapezoidal when the slots are skewed one tooth width. The measured emf shows a distorted waveform, which indicates that one side of the magnets is of lower magnetisation than the other side. The unsymmetrical strength of the magnets may be due to partial demagnetisation from a heavy load test.

The emf can be resolved into a Fourier series comprising a fundamental component and a series of odd harmonics, given by

$$e_{ph} = \sum_{j=1,3,5,\ldots} k_{sj} E_j \sin(j\frac{p}{2}\omega t) \qquad (1)$$

where p is the number of poles and ω is the rotational angular speed of the rotor in rad/s. E_j is the peak amplitude of the jth harmonic of the emf without skewed slots. k_{sj} is the skew factor for the jth harmonic.

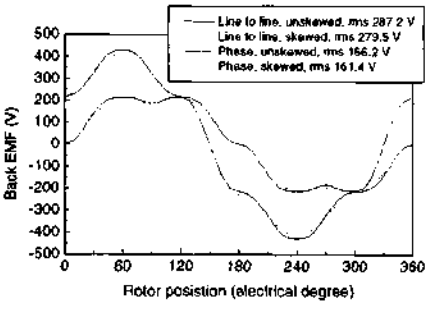

(a) Predicted back emf

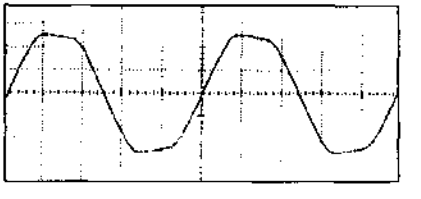

(b) Measured phase emf

Fig. 3 Comparison of predicted and measured emf for the first prototype

The synchronous reactance, X_s, consists of the armature reactance and the leakage reactance. The armature reactance can be found from incremental finite element analysis [5], while the leakage reactance can be calculated by an empirical formula.

In terms of the phase emf, e_{ph}, synchronous reactance, X_s, and phase resistance, R_a, the generator can be represented by an equivalent circuit on a per-phase basis. Thus, for a star-connected 3-phase symmetric resistive load, the load current, i_{ph}, is derived from

$$i_{ph} = \sum_{j=1,5,7,11...} \frac{k_{sj} E_j}{Z_j} \sin(j\frac{p}{2}\omega t - \alpha_j) \tag{2}$$

where

$$Z_j = \sqrt{(R_l + R_a)^2 + (jX_s)^2}$$
$$\alpha_l = \tan^{-1}(\frac{jX_s}{R_l + R_a}) \tag{3}$$

and R_l is the load resistance per phase.

Thus, the rms value of the load current is

$$I_{rms} = \sqrt{\sum_{j=1,5,7,11...} (\frac{k_{sj} E_j}{Z_j})^2 / 2} \tag{4}$$

B. *Losses and load characteristics*

The losses which affect the efficiency of the generator are the winding copper loss, stator core loss, mechanical loss predominantly from bearing and seal friction, and stray loss, due to eddy current losses in the winding and magnets.

The copper loss, p_{cu}, is the principal loss in the generator under most operating conditions. It can readily be calculated from the winding resistance at the operating temperature, and is given by

$$p_{cu} = 3I_{rms}^2 R_a \tag{5}$$

Assuming a uniform sinusoidal flux density in the lamination, the core loss, p_{fe}, can be expressed as

$$p_{fe} = p_h + p_e + p_a \tag{6}$$

where p_h is the classical hysteresis loss, p_e the classical eddy current loss and p_a the anomalous loss. These are given by

$$p_h = k_h \frac{f}{50} B_{pk}^{1.8} W_{fe}$$
$$p_e = k_e (\frac{f}{50} B_{pk})^2 W_{fe} \tag{7}$$
$$p_a = k_a (\frac{f}{50} B_{pk})^{1.5} W_{fe}$$

where k_h, k_e, and k_a are the specific hysteresis, eddy current, and anomalous losses, respectively, when the peak flux density B_{pk} is 1 T and the frequency f is 50 Hz. W_{fe} is the lamination mass. The core losses in the stator tooth and yoke are calculated separately.

The mechanical loss, p_{mec}, is given by

$$p_{mec} = T_{basf} \frac{2\pi f}{\frac{p}{2}} \tag{8}$$

where T_{basf} is the bearing and seal friction in Nm.

The stray loss, p_{stray}, was found to be 3% of the output in the first prototype. This value is used in the design optimisation.

From the resultant losses, the efficiency of the generator, η, can be obtained from

$$\eta = \frac{P_o}{P_o + p_{cu} + p_{fe} + p_{mec} + p_{stray}} \times 100 \tag{9}$$

where P_o is the output power and is given by

$$P_o = 3I_{rms}^2 R_l \tag{10}$$

For a fixed speed and operation under a balanced resistive load, the load characteristics of the generator can be obtained from equation (4) to (10). It is found that the output power reaches its maximum value when the load resistance is approximately equal to $\sqrt{R_a^2 + X_s^2}$.

Since the generator is directly coupled to the wind turbine, the operational speed varies over a range, and hence affects the no-load emf and synchronous reactance. The efficiencies for variable speed operation can also be obtained from the above equations.

C. *Thermal analysis*

The generator is a totally enclosed non-ventilated machine. As the generator is located on a tower out of doors in hot environments, its cooling depends not only upon natural convection but also radiation and solar absorption. The thermal performance is a balance of heat inputs from machine losses and solar absorption, and cooling by natural convection and radiation. A preliminary calculation showed that the heat transfer of radiation and solar absorption is approximately balanced. Thus, for simplicity the thermal analysis does not include radiation and solar absorption.

Ignoring radiation and solar absorption, the heat generated by the total loss flows to the rotor surface through conduction of the spider structure inside the stator, and convection across the air gap from the stator outer surface, and then dissipates by natural convection into the surrounding air. A lumped-parameter model for steady-state analysis is proposed to represent the complex distributed thermal parameters of the generator, as shown in Fig. 4. The lumped-parameter circuit can be solved to give the temperature rise at different locations.

D. *Performance of the non-optimised prototype*

The performance of the first prototype was predicted by the methods described above and is given in Table I. It can be seen that there is good agreement between the measured results and predicted performance, in terms of voltage, current, temperature rise and starting torque.

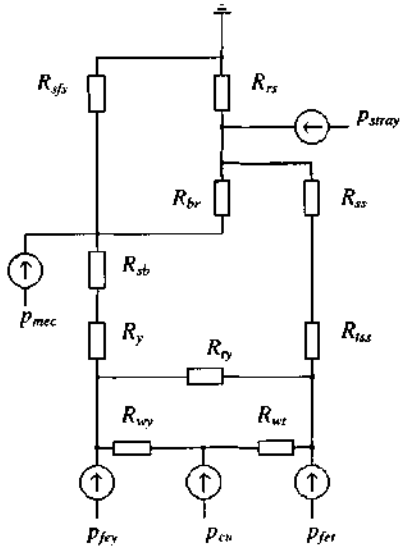

Fig.4 Lumped-parameter model for steady-state thermal analysis

R_{wt} = thermal resistance between stator winding and stator tooth
R_{wy} = thermal resistance between stator winding and stator yoke
R_{ty} = thermal resistance between stator tooth and yoke
R_{tss} =thermal resistance between stator tooth and outer surface
R_{ss} = thermal resistance between stator outer surface and rotor inner surface through convection and conduction of the air in the air gap
R_y = thermal resistance between stator yoke and inner surface
R_{sb} = thermal resistance between spider structure and bearing
R_{br} = thermal resistance between bearing and rotor
R_{rs} = thermal resistance of the rotor outer surface
R_{sfs} =thermal resistance of the supporting frame outer surface

TABLE I
PERFORMANCE OF THE FIRST PROTOTYPE

Items	Measured	Predicted
Peak cogging torque (Nm)	-	11.8
Maximum hysteresis torque (Nm)	-	18.4
Starting torque (Nm)	20~40	40
RMS current (A)	56.0	56.2
RMS voltage (V)	129.3	128.9
Power output (W)	21730	21730
Efficiency (%)	86.0	88.2
Rotor temperature rise (°C)	-	18.5
Stator winding temperature rise (°C)	57	58.5
Active mass (kg)	-	132.4

IV. DESIGN OPTIMIZATION

Based on the validated modelling procedure, an optimisation routine for the design of a 20 kW, 211 rpm direct-drive permanent magnet generator was set up. It uses eleven dimensional variables and three constraints. The three constraints are temperature rise, output power, and starting torque. The objective is to minimise the capital cost of the machine including materials, power loss, supporting structure and wind speed variations. It is noted that the cost optimisation effectively minimises the active mass due to the high cost of the tower and site installation. The parts cost of the machine is small compared with the total cost (eg the cost of rare earth magnets is only about 1% of the total cost). The running cost was also found to be small compared with the capital cost.

It is very important to provide an initial feasible design for the optimisation process, which can narrow the design space and therefore save computation time. The design data for the first prototype was used for the initial design.

Design optimisations for several numbers of poles, and several lamination and magnet materials were performed. The design results are given in Table II-IV. For a fixed number of poles, eg 48, the design with short stack length shows a minimum active mass or total cost. When the stack length is fixed, the active mass decreases with an increase of the number of poles. It has been found that a better grade of lamination material helps to meet the starting torque (hysteresis torque) requirement, while a better grade of magnet material increases output power. The most favourable design is a 60-pole machine with Ly-core 130 lamination and N35SH magnet. However, this design has a large diameter of 0.9 m.

V. THE SECOND PROTOTYPE DESIGN AND TEST

As manufacturing methods placed an upper limit on the outer-rotor drum diameter, a 36-pole wind generator was selected for the second prototype. Values of the principal design details are given in Table V.

TABLE II
20 KW GENERATOR DESIGN OPTIMIZATION FOR DIFFERENT NUMBER OF POLES
(LY-CORE 220 LAMINATION AND N27SH MAGNET)

Poles	36	40	48	54	60
Winding temperature rise (°C)	115	122	124	130	130
Efficiency (%)	87.1	86.5	86.7	86.7	86.5
Outer diameter (10^3 m)	689	691	795	906	901
Overall length (10^3 m)	274	263	219	196	190
Active mass (kg)	115	106	94	86	82

TABLE III
20 KW GENERATOR DESIGN OPTIMIZATION FOR DIFFERENT LAMINATION MATERIALS
(60 POLES AND N27SH MAGNET)

	Grade	Ly-core 220	Ly-core 130	Nippon 35H
Lamination	Cost (A$/kg)	2	4	4
	Core loss (W/kg)	2.5	1.3	1.0
Winding temperature rise (°C)		130	130	130
Efficiency (%)		86.5	87.1	87.2
Hysteresis torque (Nm)		9.2	4.1	3.4
Outer diameter (10^3 m)		901	913	877
Overall length (10^3 m)		190	185	187
Active mass (kg)		82	79	77

TABLE IV
20 KW GENERATOR DESIGN OPTIMIZATION FOR DIFFERENT MAGNET MATERIALS
(60 POLES AND LY-CORE 220 LAMINATION)

	Grade	N27SH	N33SH	N35SH
Magnet	Cost (A$/kg)	140	150	160
	Remanence (T)	1.06	1.15	1.19
Winding temperature rise (°C)		130	130	130
Efficiency (%)		86.5	86.9	86.9
Hysteresis torque (Nm)		9.2	9.7	9.6
Outer diameter (10^3 m)		901	1017	976
Overall length (10^3 m)		190	182	183
Active mass (kg)		82	81.7	80

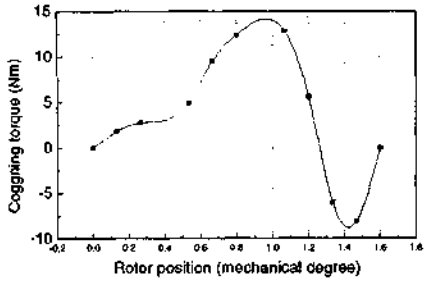

Fig. 5 Cogging torque as a function of rotor position

TABLE V
PRINCIPAL DESIGN DETAILS OF THE SECOND PROTOTYPE

Nominal power	20 kW
Nominal speed	211 rpm
Number of poles	36
Number of phases	3
Outer diameter	610 mm
Overall axial length	298 mm
Air gap	1.6 mm
Lamination material	Ly-core 22
Magnet material	N35SH Nd-Fe-B
Magnet thickness	3.5 mm
Active mass	112 kg
Resistance per phase at 20 °C	0.1764 Ω
Synchronous inductance per phase	4.48 mH
Synchronous reactance at 211 rpm	1.783 Ω
No-load phase emf	209 V
Voltage at 20 kW output	189 V
Current at 20 kW output	35.1 A
Efficiency at 20 kW output	91.6 %
Maximum power output at 211 rpm	28.1 kW

The cogging torque is minimised when the magnet arc ratio is 0.7 and the slot opening width is 3.7 mm. Fig. 5 shows the cogging torque without skewed slots as a function of rotor position. With skewed slots for one tooth width, the peak cogging torque is 5.8 Nm. The hysteresis torque is 8.4 Nm. Therefore, the starting torque of the generator is 16.2 Nm including 2 Nm for bearing and seal friction. The measured staring torque of the second prototype is 20 Nm.

Fig. 6 shows the cross section of the generator with its flux lines at no-load. The predicted back emf at no-load is shown in Fig. 7. Fig. 8 shows the load characteristics of the generator at 211 rpm. For a maximum output power, the load resistance per phase is about 2.24 Ω. The voltage and current waveforms for the maximum output power are shown in Fig. 9. It is noted that the current for a heavy load tends to be inductive since the synchronous reactance is much larger that the winding resistance. Fig. 10 shows the performance as a function of speed. The output power from the wind turbine is proportional to the shaft speed cubed for the speed up to nominal speed. The generated voltage is proportional to the speed squared. Therefore the current is proportional to the speed squared when the speed is less than the nominal speed. When the speed is higher than the nominal speed, the load current keeps constant.

To test the second prototype in the laboratory the direct-drive permanent magnet generator was driven by a Mazda internal combustion engine. Fig. 11 shows the measured open-circuit voltage waveform at no-load, which agrees well with the predicted waveform shown in Fig. 6. While varying symmetrical 3-phase resistive load, the voltage, current, and input power were recorded for different engine speeds. Two sets of 3-phase resistors were connected either in star or delta to give 3, 6, 9 and 18 Ω for the load resistance. Fig. 12 and 13 show the measured output power and efficiency of the generator as a function of speed, respectively.

The load characteristics at 211 rpm can be extracted from the test data and are shown in Fig. 14. When the output power reaches 20 kW at 211 rpm, the phase voltage is 202 V, the efficiency 94 %, and the load current 33 A. The measured voltage and efficiency are slightly higher than the predicted values shown in Table V for the following reasons:

- An average value for the remanence of the magnets was used in the design, which may be less than the actual values for the delivered magnets.
- An ambient temperature of 50 °C was assumed in the design as the generator was assumed on the tower. This value is higher than that in the laboratory. Therefore, the operation temperature of the magnets was higher than the test condition, which results in a lower remanence of the magnets.
- The stray loss was assumed to be 3% of the output power, which may be too high for the second prototype.

The test results of the generator with a resistive load confirm the satisfactory operation of the generator. The direct-drive generator is currently installed with a two-blade turbine on a 36m tower at Murdoch University, to conduct full site testing. Figs. 15 and 16 show the direct-drive generator mounted on the main frame and on the tower, respectively.

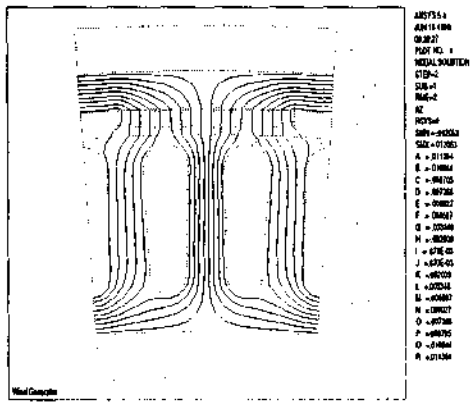

Fig. 6 Flux line at no-load

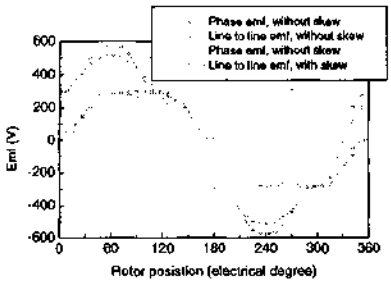

Fig. 7 Predicted no-load emf waveforms at 211 rpm

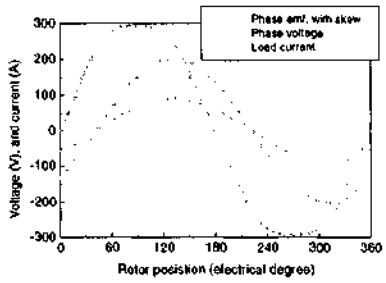

Fig. 9 Voltage and current waveforms for maximum output power at 211 rpm

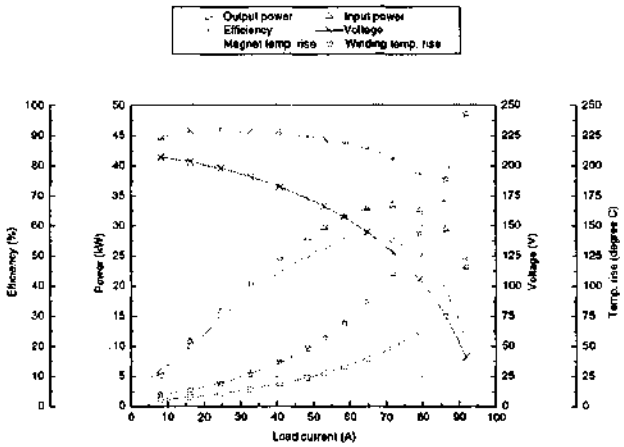

Fig. 8 Predicted load characteristics at 211 rpm

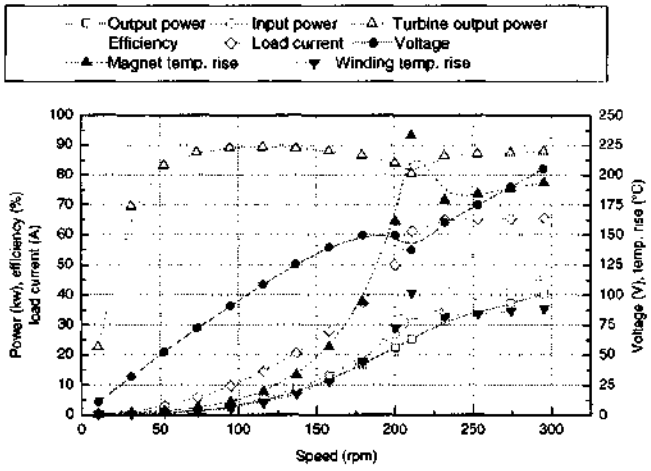

Fig. 10 Predicted performance against speed under resistive load

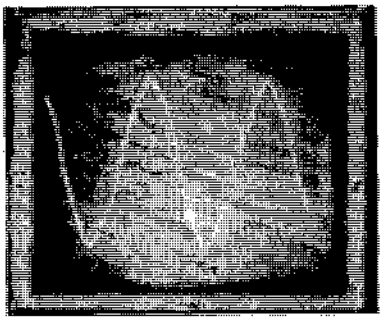

Fig. 11 Measured open-circuit voltage waveform

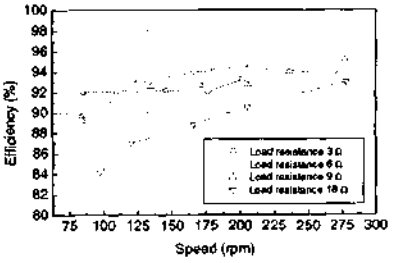

Fig. 13 Measured efficiency against speed

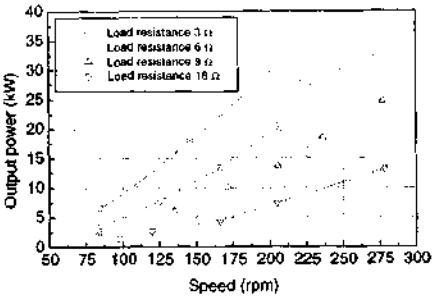

Fig. 12 Measured output power against speed

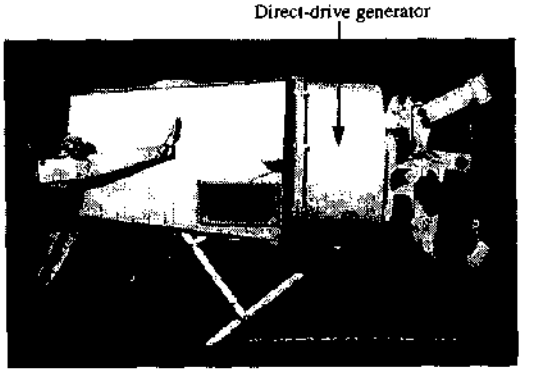

Fig. 15 Direct-drive generator mounted on the main frame

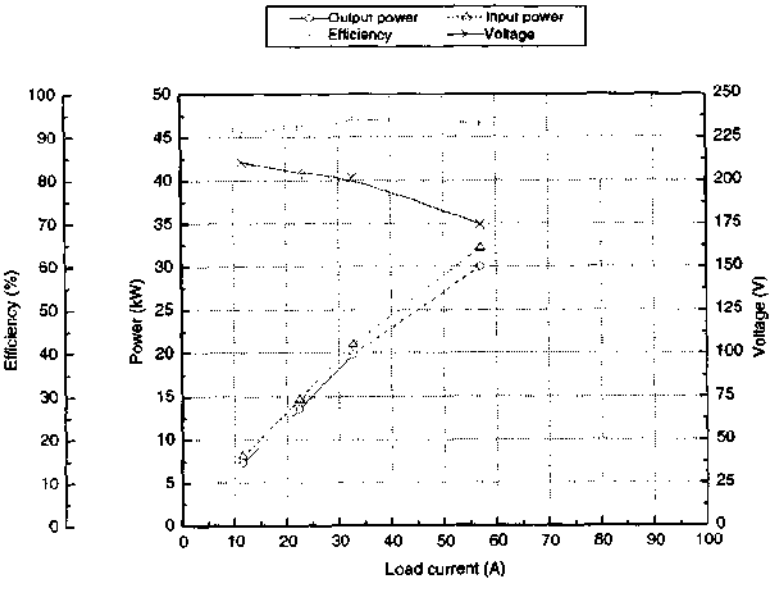

Fig. 14 Measured load characteristics at 211 rpm

Fig. 16 Direct-drive generator on the tower

VI. Conclusion

The cogging torque, back emf, synchronous reactance and iron loss of a direct-drive permanent magnet wind generator were calculated by using a finite element analysis. Combined with an equivalent circuit and a lumped-parameter thermal model, the analysis of the performance under a balanced resistive load was presented and validated by examining the non-optimised 20 kW prototype.

A design optimisation routine was applied to study a range of designs with different number of poles, different lamination and magnet materials. The design of a 36-pole machine was finalised and built, which has a larger diameter and shorter axial length than the previous prototype. Test results with a resistive load have confirmed satisfactory operation of the generator. Its active mass is smaller, it has a lower starting torque, and it is more efficient, compared to the previous prototype.

Acknowledgment

The authors would like to thank Jianyi Chen at Curtin University of Technology, for providing them with test results of the previous prototype. Thanks also go to Howard Lovatt at CSIRO and Peter Watterson at UTS for discussions.

References

[1] B.J. Chalmers, W. Wu, E. Spooner, "An axial-flux permanent-magnet generator for a gearless wind energy system," *IEEE trans. on Energy Conversion*, Vol. 14, No. 2, June 1999, pp251-257.

[2] E. Muljada, C.P. Butterfield, Y. Wan, "Axial-flux modular permanent-magnet generator with a toroidal winding for wind-turbine applications," *IEEE Trans. on Industry Applications*, Vol. 35, No. 4, July/August 1999, pp831-836.

[3] V. S. Ramsden, "Application of rare-earth magnets in high-performance electric machines," *15th International Workshop on Rare-Earth Magnets and Their Applications*, Dresden, 30 August-3 September, 1998, pp623-642.

[4] J.Y. Chen, C.V. Nayar, "A multi-pole permanent magnet generator direct coupled to wind turbine," *International Conference on Electrical Machines*, Istanbul, Turkey, 2-4 September 1998, pp1717-1722

[5] M. Gyimesi, D. Ostergaard, "Inductance computation by incremental finite element analysis," *IEEE Trans. Magnetics*, Vol. 35, No. 3, May 1999, pp1119-1122.